Maturation of adenovirus primes the protein nano-shell for successful endosomal escape

Denning, D.; Bennett, S.; Mullen, T.; Moyer, C.; Vorselen, D.; Wuite, G. J.L.; Nemerow, G.; Roos, W. H.

published in
Nanoscale
2019

DOI (link to publisher)
10.1039/c8nr10182e

document version
Publisher's PDF, also known as Version of record

Nanoscale

PAPER

View Article Online
View Journal | View Issue

Cite this: *Nanoscale*, 2019, **11**, 4015

Maturation of adenovirus primes the protein nanoshell for successful endosomal escape†

D. Denning,[a,b] S. Bennett,[c] T. Mullen,[c] C. Moyer,[c] D. Vorselen,[b] G. J. L. Wuite,*[b] G. Nemerow*[c] and W. H. Roos[a]

The ability of adenoviruses to infect a broad range of species has spurred a growing interest in nanomedicine to use adenovirus as a cargo delivery vehicle. While successful maturation of adenovirus and controlled disassembly are critical for efficient infection, the underlying mechanisms regulating these processes are not well understood. Here, we present Atomic Force Microscopy nanoindentation and fatigue studies of adenovirus capsids at different maturation stages to scrutinize their dynamic uncoating properties. Surprisingly, we find that the early intermediate immature (lacking DNA) capsid is mechanically indistinguishable in both break force and spring constant from the mature (containing DNA) capsid. However, mature and immature capsids do display distinct disassembly pathways, as revealed by our mechanically-induced fatigue analysis. The mature capsid first loses the pentons, followed by either long-term capsid stability or abrupt and complete disassembly. However, the immature capsid has a stable penton region and undergoes a stochastic disassembly mechanism, thought to be due to the absence of genomic pressure. Strikingly, the addition of the genome alone is not sufficient to achieve penton destabilization as indicated by the penton stability of the maturation-intermediate mutant, G33A. Full penton destabilization was achieved only when the genome was present *in addition* to the successful maturation-linked proteolytic cleavage of preprotein VI. Therefore these findings strongly indicate that maturation of adenovirus in concert with genomic pressure induces penton destabilization and thus, primes the capsid for controlled disassembly. This latter aspect is critical for efficient infection and successful cargo delivery.

Received 17th December 2018,
Accepted 11th February 2019

DOI: 10.1039/c8nr10182e

rsc.li/nanoscale

Introduction

The ability of adenoviruses (AdVs) to infect many different species and tissues has led to a widespread interest not only in their biology and pathogenicity, but also in possible applications of these viral nanoparticles. This interest includes for instance the objective of fighting adenovirus infection as well as the use of AdV for therapeutic applications, *e.g.* vectors in gene and vaccine therapy.[1,2] However, a lack of fundamental knowledge and understanding regarding key steps in the infectious life cycle of the virus have hampered such efforts. Successful maturation of adenovirus as well as its controlled disassembly is critical for efficient infection *in vivo*. Yet the underlying mechanisms regulating these processes are not well understood. Non-enveloped viruses generally undergo major structural rearrangements during their development from immature capsids to mature capsids. This process often requires proteolytic processing of capsid preproteins that sometimes drastically change their mechanical properties.[3–5] In the case of the enveloped retrovirus HIV, a stiffness switch was identified during proteolytically-induced maturation which correlated with infectivity, highlighting an intricate link between viral mechanics and infectivity.[3]

AdVs are non-enveloped, pseudo-T = 25 icosahedral viruses which are ~90 nm in diameter. The particles are composed of three major and four minor (cement) capsid proteins, three core proteins, a terminal protein (TP) and the AdV protease (AVP).[6,7] During maturation, proteolytic cleavage of multiple capsid preproteins transforms the immature, non-infectious virus particle into a mature, infectious virion.[7] More specifically, the most accepted model of AdV assembly and maturation begins with an 'empty' immature intermediate capsid (IC), containing all precursor capsid proteins and the L1 52/55K scaffold protein.[8–10] The genome is then recognized and packaged *via* a largely unknown process, followed by the

[a]*Moleculaire Biofysica, Zernike Instituut, Rijksuniversiteit Groningen, The Netherlands*
[b]*Natuur- en Sterrenkunde and LaserLaB, Vrije Universiteit Amsterdam, The Netherlands. E-mail: gwuite@nat.vu.nl*
[c]*Department of Immunology and Microbiology, the Scripps Research Institute, La Jolla, CA, 92037, USA. E-mail: gnemerow@scripps.edu*
†Electronic supplementary information (ESI) available. See DOI: 10.1039/c8nr10182e

cleavage of six precursor (three capsid and three core) proteins and the scaffold protein.[11,12] The scaffold protein is present at ~100 copies in immature particles as compared with 0 copies in the mature virus and is thought to contribute significantly to the stability of the empty immature virus.[7,13]

Much of what is currently known about the maturation of AdV is derived from experiments with the human AdV-C2 (HAdV-C2) temperature-sensitive mutant *ts*1, which fails to package the AVP responsible for cleavage of the capsid preproteins.[14] This mutant does package DNA and it contains all precursors proteins, including the L1 52/55K scaffold protein. While *ts*1 particles have been invaluable for identifying the importance of proteolytic processing during AdV maturation, insights into any particular intermediate stage in the maturation pathway or indeed the role of each cleavage site during maturation of AdV cannot be deduced from studying these particles. Thus, there remains a big gap in our knowledge of maturation and other model systems are desired. Recently, a single point mutant of precursor protein VI (pVI), G33A, was generated.[15] The pVI-G33A virus has decreased AVP cleavage of the N-terminus domain of pVI that results in the presence of an intermediate preprotein VI (iVI).[15] The mutant virus, G33A, contains ~50% iVI molecules and exhibits a 2–4 fold reduction in infection with respect to the wild-type HAdV-C5 virus. In addition, it displays reduced ability to lyse the endosome after entry into the cell. This was linked to a reduction in protein VI (VI) exposure, since VI mediates the membrane lysis which is critical for viral escape out of the endosome and thus, to continue infection.[16] Successful uncoating of AdV begins with fiber shedding and release of pentons in the acidified endosome.[17] Since recent structural data indicates that protein VI is located beneath each hexon, including peripentonal hexons, it follows that removal of the adjacent pentons is critical for exposure of VI.[17–20]

Atomic force microscopy (AFM) is a commonly used analytical tool to elucidate the material properties of individual virus particles.[4,21–24] In the case of AdV, nanoindenation by AFM was used to study how the elastic properties of AdV are modulated by interactions with host proteins[25] highlighting the link between its mechanics and infectivity. Furthermore, a high internal pressure (~30 atm) of the AdV core was estimated following AFM experiments using the *ts*1 mutant and multivalent cations.[5] This internal pressure was proposed to facilitate the stepwise disassembly of the virus. AdV was also used in a correlative AFM-fluorescence microscopy approach to study genome delivery,[26] and AdV's strength turned out to be modifiable by a single point mutation in a precursor protein.[27]

Here, we use wild type (WT), the G33A mutant (G33), and immature AdV capsids (IC) to study the mechanics and disassembly of AdV at different stages of maturation. By employing the capability of AFM to obtain both spatial and temporal information, we are able to elucidate key aspects of the mechanically-induced virus disassembly pathway. Though the wild type and immature particles are mechanically indistinguishable, they exhibit markedly different disassembly pathways that primarily result from the influence of the genome. While the maturation-intermediate particle G33A has a similar disassembly pathway to the wild type, this mutant was found to release half the number of pentons which likely results in this particle becoming trapped in the endosome during infection. Taken together, the findings of this study highlight that maturation of AdV *in concert* with genomic pressure results in penton destabilization, thereby priming the capsid for controlled disassembly.

Results and discussion

Nanoindentation of AdV at different stages of capsid maturation

The mechanical properties of the IC, the WT and the G33, representing separate stages of maturation and assembly, were analysed by AFM. The IC particles contain all precursor proteins and the L1 55/52K scaffold protein, however they lack the majority of the dsDNA genome.[28] WT capsids contain a fully packaged genome, and have undergone complete maturation. In these capsids the adenoviral protease (AVP) has successfully cleaved all precursor protein target sites. In the G33 capsid, however, AVP has cleaved all precursor capsid proteins with the exception of ~50% of the N-terminus cleavage sites of preprotein VI, leading to an intermediate protein VI (iVI).[15] Schematic representations of the three capsids are shown in Fig. 1a. Each capsid was investigated using AFM nanoindentation to reveal their mechanical properties. First, the capsids were imaged and then a force–distance curve (FDC) was performed *via* nanoindentation at the center of the particle.[29] Afterwards, another image was taken to visualize the damage inflicted upon the capsid. Fig. 1b shows the height image of a WT capsid before and after a typical nanoindentation experiment. A line profile of the capsid before and after indentation is also shown, which in this case reveals that the damage to the capsid is significant, and its height has been reduced by approximately one half. There are features appearing on the glass surface next to the capsid after indentation, which have a nearly uniform size, as seen in the after image. A zoom in on the line profile after indentation reveals these features have the same height as a hexon trimer, a major capsid protein, which is in agreement with previous observations in AFM nanoindentation studies of AdV.[25]

The spring constant (elastic property) and break force (resilience to fracture) of each capsid was also measured from the FDC (Fig. S1a and b†). Surprisingly, we detected two distinct populations within the data for the break forces and spring constants for the capsids, as shown in more detail by the example of the WT data in Fig. 2a. The distinction was found to originate from the size of the tip radius (R_{tip}). The use of a blunt tip (R_{tip} ~ 35 nm – dataset includes tips with R_{tip} = 40 and 33 nm) resulted in a break force and spring constant approximately double that of a sharp tip (R_{tip} ~ 20 nm – dataset includes tips with R_{tip} = 18, 25, 17 and 22 nm). To investigate the mechanism underlying this different behaviour, we studied the force-indentation curves (FICs) more closely, as

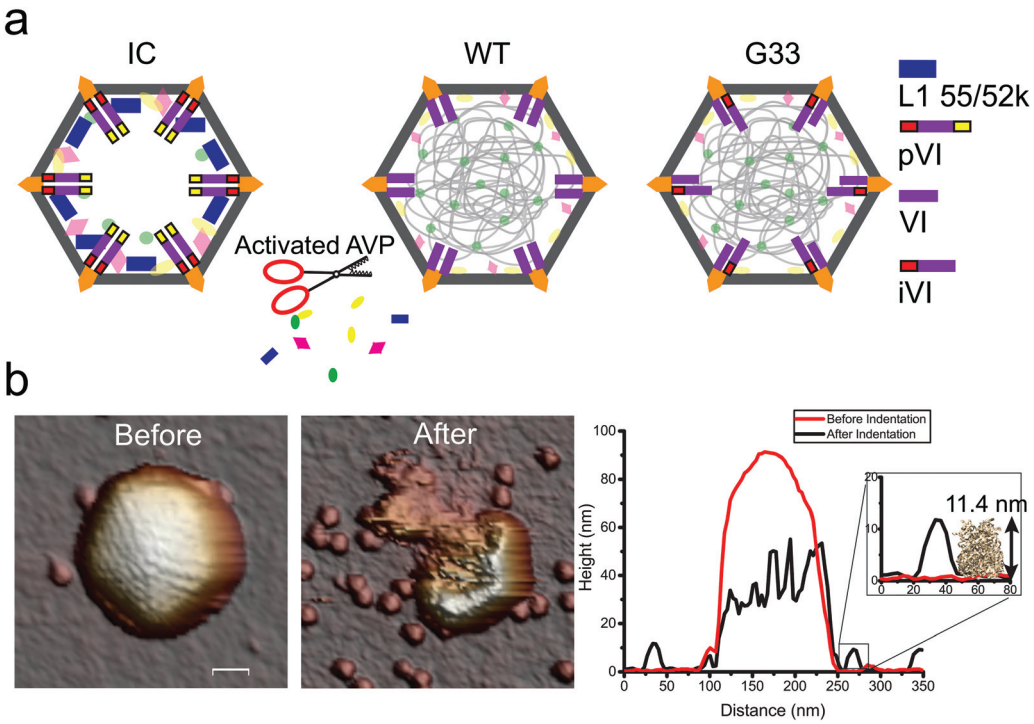

Fig. 1 Nanoindentation of immature capsid (IC), mature Ad5 (WT) and G33 mutant. (a) Schematic of each capsid used in this study. The proteins not listed in the legend but which appear in the schematics represent the various capsid and core minor proteins of AdV. (b) AFM image of a WT capsid before and after an indentation, and line profile showing the corresponding reduction in height. The inset shows the presence of hexon trimers on the surface (PDB code, 1VSZ). Scale bar is 40 nm. Maximum *z*-height in before and after image is 95 nm and 66 nm, respectively.

shown in Fig. 2b. In the case of the blunt tip, the initial slope of the indentation curve is steeper (higher spring constant) and the particle breaks at a higher force than during indentation performed with a sharp tip. In addition, we frequently observed minor breaks in the indentation response due to the sharp tip, as highlighted by the black arrow in Fig. 2b. In the case of WT capsids, the probability of minor breaks occurring in the indentation curve when using a sharp tip is 0.7, as opposed to 0.05 with a blunt tip. This behaviour is independent of the capsid type investigated, as a similar trend in the probability of breaks between indentation curves using sharp and blunt tips was observed for ICs and G33 capsids. There is a higher local pressure on the capsid during indentation with a sharp tip, resulting from the smaller contact area for a given force. This likely induces local fractures during indentation, as visualised by the breaks. In contrast, indenting with a blunt tip likely results in a more uniformly distributed pressure across the capsid due to a larger contact area and thus, the whole capsid behaves stiffer and more resilient. It means that the capsid fractures during indentation with a sharp tip due to higher local pressure, *versus* a global capsid collapse during indentation with a blunt tip due to a more evenly distributed pressure.

To understand the resultant capsid structure after indenting with a sharp and blunt tip, we considered the recorded height at the end of indentation. This is designated in Fig. 2b as the maximum indentation, illustrated by the steep slope characteristic for (nearly) incompressible behaviour. Interestingly, the maximum indentation of capsids with a sharp tip (81.3 ± 0.8 nm; N = 27) is very similar to their measured heights from images (84.5 ± 0.4 nm; N = 95) indicating almost complete disruption of the capsid after breakage. The difference in measured heights (~3 nm) between images and indentations may be explained by the high likelihood of genomic material adhering to the glass after capsid disruption, also visible in the image after indentation in Fig. 1b. The height of the viruses before indentation with a blunt tip is also in this range (84.1 ± 0.5; N = 45), as shown by the height histogram inset in Fig. 2c. However, the maximum indentation of the capsid with a blunt tip is ~20 nm lower than this, (64.3 ± 1.6 nm; N = 24) signifying the capsid has not fully disassembled, and there is a 20 nm layer underneath the tip, as shown by the histogram in Fig. 2c. The existence of this ~20 nm layer is confirmed by the height images and line profiles taken using a blunt tip before and after indentation, as shown in Fig. S1c.† A layer of this thickness corresponds well to the combined dimensions of two capsid shell layers (capsid thickness is ~11 nm), and likely signifies a global capsid collapse. The quite drastic dependence of virus mechanics on tip size observed here is in sharp contrast to previous literature using simulations to model this effect.[30] Simulated force-indentation curves on CCMV capsids using large tip radii only observed a stiffening effect at large indentations, whereas the data presented here, albeit on a different virus, clearly shows an immediate stiffening effect (Fig. 2b). Additionally, numer-

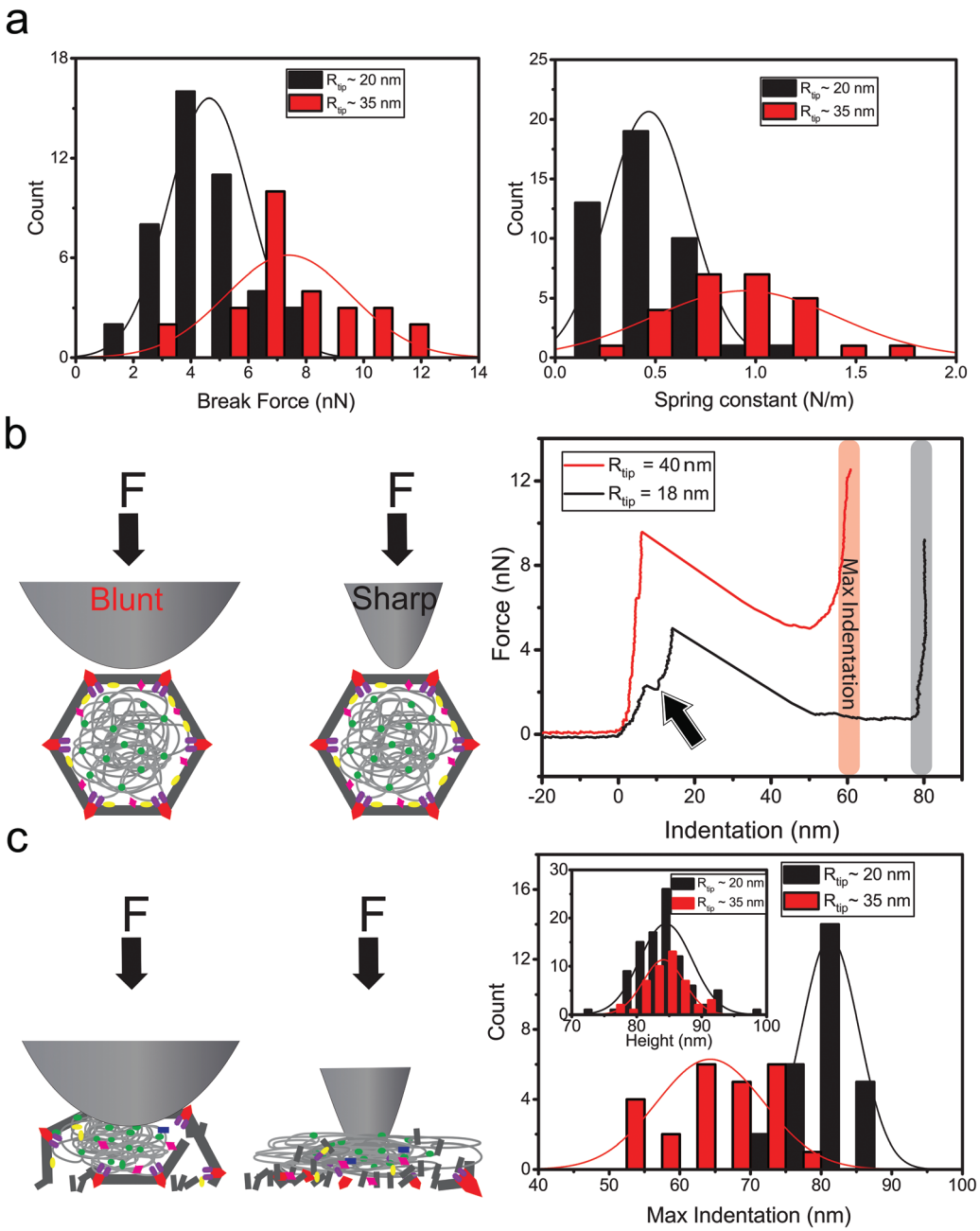

Fig. 2 Tip radius effect on measured nanomechanical properties. (a) Histogram of measured break force and spring constant for WT capsids separated into two populations representing indentations with sharp (R_{tip} ~ 20 nm) and blunt (R_{tip} ~ 35 nm) tips. (b) Schematic and representative indentation curves of a WT capsid using a sharp and blunt tip. Arrow indicates local breaks in the force curve. (c) Schematic of mechanism of indentation and histogram of the maximum indentation point of the WT capsid, using a sharp and blunt tip. Inset shows height of WT capsids as measured from height images, using a sharp and blunt tip.

ous studies on viral nanoindentation have presented indentation curves which contain the minor breaks analysed in this study.[25,31,32] Furthermore, there are some discrepancies in the literature regarding the reproducibility of nanoindentation experiments on protein nanoshells. For example, the spring constant of adenovirus reported in literature is 0.43 ± 0.01,[25] 0.46 ± 0.02,[33] 0.56 ± 0.02,[5] and 0.37 ± 0.02.[27] It is possible that the tip radius is a contributing factor to explain conflicting data on viruses in the literature. The proposed local (fracturing) *versus* global (collapsing/flattening) mechanisms of viral indentation with sharp and blunt tip respectively, are shown graphically in Fig. 2c, and henceforth these properties will be separated and termed the local and global responses, respectively.

The global break force and spring constant of each type of capsid were statistically equivalent, (Fig. S1a, b† and Table 1).

Table 1 Global and local mechanical properties of AdV capsids

	Global (blunt tip)[a]			Local (sharp tip)[b]		
Virus	N	F_{break} (nN)	k (N m^{-1})	N	F_{break} (nN)	k (N m^{-1})
IC	8	7.3 ± 0.5	1 ± 0.1	17	4.7 ± 0.3	0.43 ± 0.03
WT	27	7.3 ± 0.4	1 ± 0.1	44	4.6 ± 0.2	0.46 ± 0.03
G33	15	7.4 ± 0.3	1.1 ± 0.1	22	5.9 ± 0.3	0.55 ± 0.04

Error bars are the standard error of the mean (SEM). [a] Data taken with tips of radius – R_{tip} = 40 and 33 nm. [b] Data taken from tips of radius – R_{tip} = 17, 25, 18 and 22 nm.

In addition, the local spring constants of each capsid type were also similar (G33 capsid slightly higher than WT and IC). However, the G33 capsid had a higher local break force than both WT and IC, indicating that this capsid has an increased local mechanical resilience. Given that the N-terminus of pre-protein VI is closely associated with the interior surface of hexons,[18] it is not surprising that when 50% of the copies of this protein are uncleaved, as is the case in the G33 capsid, there is increased resilience of the virus due to reinforced hexon-IV interactions. No orientation dependence on the break force or spring constant was found for the viruses studied, as previously reported.[27] Remarkably, there was no difference locally or globally, in the spring constant or break force, between the WT mature capsid and the IC. This is surprising since the protein composition and structure, as well as the DNA content of these capsids are markedly different. It also distinguishes the IC from the *ts*1 mutant, which has a lower spring constant and break force than WT mature Ad5.[5,33] As it has been determined that the IC has ~50% more scaffold proteins than the *ts*1 mutant, this could explain the increased resilience of the IC and the observed differences.[13,34]

Capsid-type dependency on disassembly pathways

The similarities in the elastic properties and mechanical resilience of WT and ICs as described above, raised the question as to whether these viruses also have a similar capsid disassembly pathway. To address this question, a fatigue analysis was undertaken in which the capsid is imaged over a long time period at a constant low force of ~150 pN that ultimately induces disassembly by fatigue.[21,35] The disassembly process of adenovirus is tightly regulated and can be recapitulated by the input of energy by mechanical fatigue, and similarly thermal or chemical energy as previously shown.[33] To achieve capsid stability on the surface such that long scanning times (and thus mechanical fatigue measurements) were possible, a charged mica surface was used. This resulted in predominantly 3-fold axis orientations, presumably due to the larger surface area of the 3-fold face forming a stable electrostatic interaction with the mica surface. In the case of the WT capsid, pentons were released from the capsid as highlighted by arrows in Fig. 3a, yet in typical cases, the capsid structure remained mostly intact even after a very long period of scanning (up to ~300 minutes). In only 1 of 4 virions here did the capsid disassemble within the given time duration, as shown by the virus height data over time in Fig. 3b, yet all 4 viruses had released their pentons. This is in sharp contrast to the disassembly behaviour seen previously for Ad5 WT,[35] where after penton release the capsid quickly disassembled. The discrepancy between the two studies could well be due to sample preparation. In the current study capsids were analysed directly after isolation from infected cells whereas in the earlier reported study, the capsids were subjected to a freeze–thaw cycle. Therefore, as a control, we put the capsids through a freeze–thaw cycle and repeated the fatigue experiment. The freeze–thaw capsids exhibited almost identical fatigue behaviour as the capsids in the previous study, as shown in Fig. S2a.† They released pentons and disassembled quickly thereafter into hexons. In contrast, the observed long-term stability of the pentonless WT capsids that did not undergo a freeze–thaw cycle, correlates more closely with the infection pathway *in vivo* and is consistent with the fact that after penton loss in the endosome, adenovirus must still protect the genome on its journey towards the nuclear pore complex.[16] Moreover, forces mediated by kinesin-1 are needed to fully disrupt the capsid and allow for full genome uncoating to achieve nuclear access.[36]

Disassembly of the ICs appears to be random, without a preferred pathway. In all cases a defect appeared in a random region of the capsid and propagated from the initial nucleation site, an example of which is shown in Fig. 3a. Once triggered, disassembly occurs slowly over time, indicating that the absence of the full genome (and thus the absence of high internal pressure) leads to a slow, stochastic disassembly mechanism. The stochastic disassembly of the IC can be described by fatigue-induced delocalized defects and propagation of the defect into a crack in the capsid. This is distinctly different from the WT/mature capsid that disassembles *via* penton release. Penton release in AdV is a requirement for protein VI exposure and resultant endosome rupture.[16] Therefore, efficient penton release is crucial for effective infectivity. Only rarely (~30% probability of a penton releasing after 1 hour scanning, compared to 95% for WT) were pentons released during disassembly of the IC. The *ts*1 mutant however, which contains all precursor proteins similar to the IC used in this study, does disassemble through penton release.[35] Nevertheless, the *ts*1 mutant contains a genome (and pressure, albeit reduced as compared with WT). Therefore, the lack of genomic pressure can be concluded as the mechanism underlying the distinctly different disassembly mechanisms of the WT and IC, as well as a strong contributor of penton destabilization. Previous fatigue studies of WT Ad5 suggested that proteolytic cleavage during maturation as well as genomic pressure may result in the destabilization of pentons.[35] The data reported here strongly indicates that this is the case, with genomic pressure contributing more to penton destabilization than perhaps previously suspected. These results underscore the role of the genome-induced pressure in AdV that results in fixed disassembly pathway through penton release.

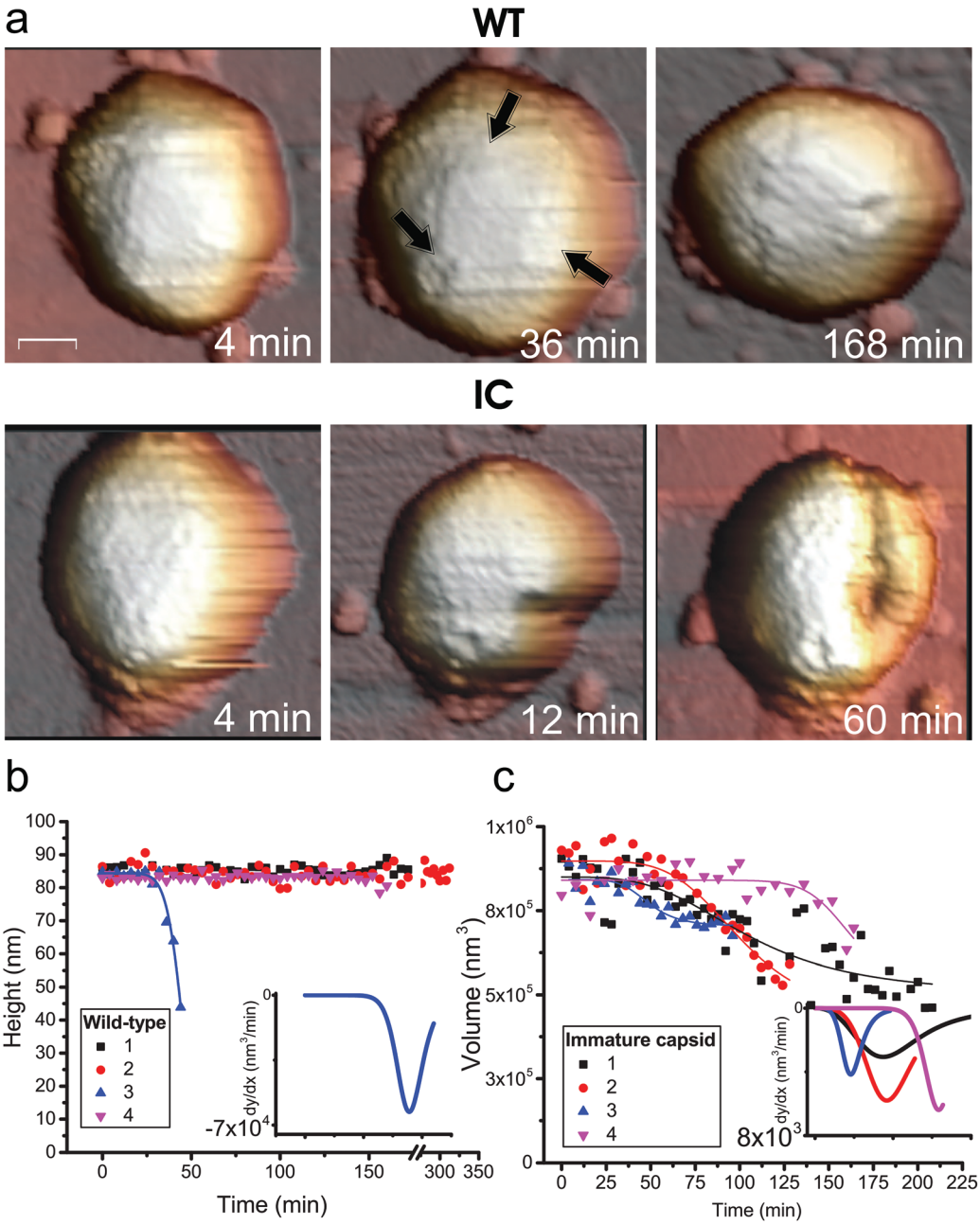

Fig. 3 Fatigue analysis of mature WT capsid and immature capsid. (a) Images at different scan times for both WT and ic reveal different disassembly pathways, where WT capsids lose pentons (arrows), but are typically stably imaged for long periods after penton release. ICs disassemble slowly *via* delocalized defects induced in the capsid and subsequent crack propagation. Scale bar is 40 nm. Maximum *z*-height for WT and IC images are 90 nm and 87 nm, respectively. (b, c) Height *vs*. time and volume *vs*. time graphs for the WT capsid and EC, respectively. Solid lines represent best fit of the logistic sigmoid function. Inset of (b, c) shows the first derivative of each sigmoid fit.

The disassembly dynamics of the G33 capsid was investigated using the same fatigue experiment. The G33 capsid underwent a similar disassembly pathway as the WT capsid, consisting of penton release followed by either a stable capsid or a capsid undergoing full disassembly. Representative movies of disassembly for each capsid are provided as ESI.† The height images in Fig. 4a illustrate the disassembly of one G33 capsid *via* penton release (highlighted *via* arrows) and subsequent collapse. To quantify the disassembly temporal dynamics of the different capsid types, the capsid height cannot be used since even after a crack is induced in the ICs, the height can remain the same if the crack is not localised at the top of the capsid. Therefore, the capsid volume was chosen to investigate the rate of the disassembly process of WT, IC and G33. The volume data of the capsids were fitted with a logistic (sigmoid) function to determine the behavioural trend

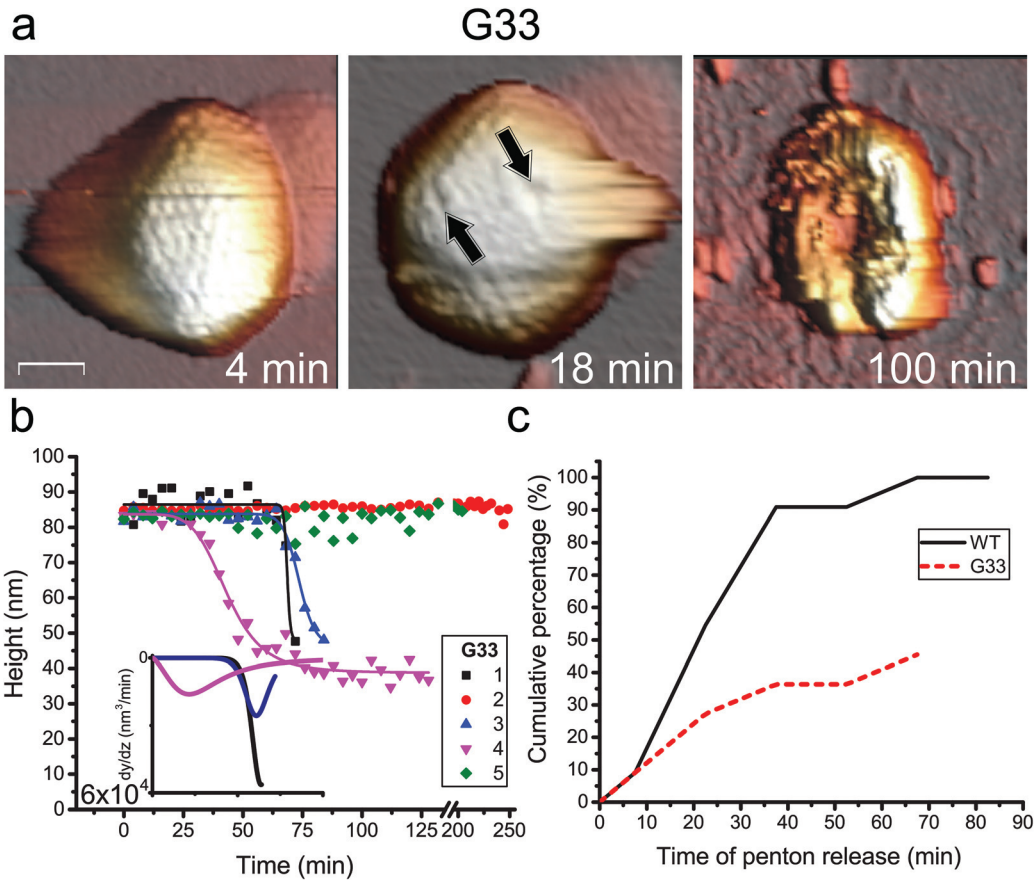

Fig. 4 G33 disassembly and penton release. (a) G33 disassembles in a similar pathway to WT. Scale bar is 40 nm. *z*-Scale bar for 4, 24 and 100 min are images 91, 93 and 53 nm, respectively. (b) Height *vs.* time graph of G33. Solid lines represent best fit to logistic sigmoid function. Inset of (b) shows the 1st derivative of each sigmoid fit. (c) Cumulative percentage of pentons released for WT relative to g33–55% less pentons are released for G33.

of volume over time. The 1st derivative of the fitted sigmoid was then calculated in order to determine the maximum speed of disassembly (nm^3 per minute), as measured by the peak of the 1st derivate. The ICs display a maximum speed of disassembly of $\sim 5 \times 10^3$ nm^3 per minute ($n = 4$; inset of Fig. 3c). The single fresh WT capsid disassembled at a rate of 6×10^4 nm^3 per minute (inset of Fig. 3b) and the G33 capsids disassembled at $\sim 3 \times 10^4$ nm^3 per minute ($n = 3$; inset of Fig. 4b). It is interesting to note that the freeze–thaw WT capsids also have a similar speed of disassembly (3×10^4 nm^3 per minute ($n = 4$; inset of Fig. S2a†). This reveals that the disassembly rate of the DNA-containing G33 and WT (fresh/frozen) capsids ($n = 8$) is significantly higher than disassembly of the IC which lacks the majority of its DNA ($n = 4$). Therefore, it can be deduced that the genomic pressure of adenovirus has an accelerating influence on capsid disassembly.

It is not obvious that the fatigue behaviour of the G33 and WT is similar. It was anticipated that there would be a stronger resistance to mechanically-induced fatigue for G33 with respect to WT due to the observed increase in mechanical resilience of G33, as seen from nanoindentation data (Fig. S1a and b†). However, the similar resistance to disassembly of WT and G33 capsids and the abrupt disassembly in cases where the capsids do fall apart, is consistent with the fact that both capsids contain the full genome inside. Therefore, they likely have a similar internal pressure, since the DNA-condensing polypeptides of preprotein VII and protein mu are present and are cleaved.[15] Still, if both capsids have a similar internal pressure and uncoating dynamics, this does not explain the observed reduction in infection *via* endosomal escape of G33. To address this conundrum, the role of dynamic penton release was investigated, as shown in Fig. 4c. The time of penton release was very similar between WT and G33 capsids; after ~40 minutes scanning, almost no further change in penton release was observed for both viruses, as indicated by saturation of the cumulative probability of penton release. It is interesting to note also that the average time of release of the first penton is similar between WT (22 ± 12 min) and G33 (21 ± 11 min). Strikingly, however, G33 was observed to release ~50% less pentons during the driven fatigue experiments than WT capsids, correlating well with the observed differences in infectivity between the two types of particles. As described earlier in the text, 50% of the N-terminus cleavage sites of protein VI are unprocessed in G33, resulting in ~180 extra iVI-hexon interactions compared to the WT capsid, many of which are surrounding the peripentonal region. Furthermore, the

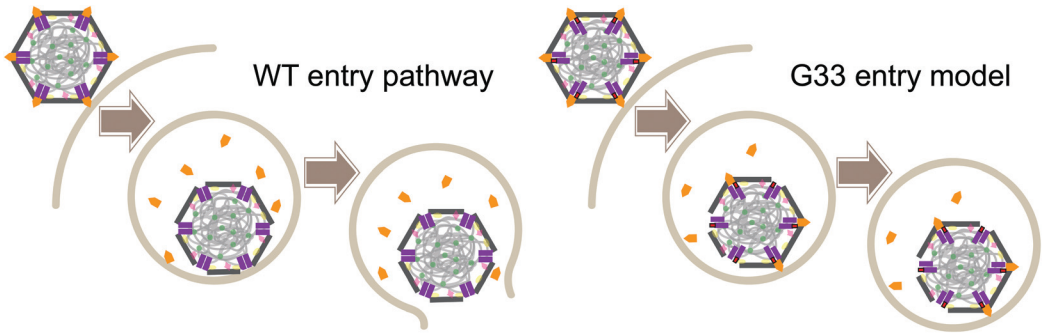

Fig. 5 Schematic of early infection stage for WT and G33 mutant. Destabilization of WT pentons occurs after binding to the virus and are subsequently released in the endosome allowing for protein VI exposure and endosomic rupture. G33, however, has more stable pentons thus reducing protein VI exposure in the endosome and preventing escape and further infection.

similarity in the time (and number) of pentons released for fresh and frozen WT capsids as shown in Fig. S2b,† highlights the importance of protein VI cleavage in overall penton stability. While protein VI density has not been clearly verified in structural studies, a recently published study has resolved the close proximity of the N-terminus of protein VI (pVIn) and the penton base and is shown in Fig. S2c.†[37] If we estimate that each hexon at the peripentonal region contains a single pVI molecule, that means there are a maximum of ~60 (12 × 5) pVI molecules in total near the vertices and some of them will get exposed by penton release. This extra stability of the penton region is supported by the observed increase in local mechanical resilience of G33 from this study. Taken together with the substantial reduction in G33 particle production shown previously,[15] the data points towards a stabilization of penton region of the G33 capsid resulting in a lower probability of protein VI exposure and thus, a reduction in endosome disruption,[38] as described graphically in Fig. 5. The stabilization of the vertex region of G33, has properties of a maturation-intermediate, and is reminiscent of virus particles complexed with human alpha defensin 5 (HD5). HD5 is a microbial protein which blocks AdV infection by stiffening and stabilizing the vertex region of AdV.[25] Spatial information from the mechanical fatigue of single viruses allows for the visualization of its disassembly pathway. Our findings indicate that the reduction of infectivity of G33 can be explained, in part, through the lack of VI exposure during penton release. A reduction in VI exposure results in decreased endosomal lysis, a step that is critical for productive infectivity.

Conclusion

We performed single particle analyses of adenovirus shells representing different stages of capsid maturation. We demonstrated the influence of AFM tip radius on the mechanical response of the particles. Using tips with defined sizes, we demonstrated that maturation of adenovirus influences its mechanical behaviour and fatigue-induced disassembly pathway in an unexpectedly complex manner. A lack of genomic pressure in immature capsids results in a stable penton region and stochastic disassembly of the capsid. However, the addition of the genome alone is not enough to achieve penton destabilization, as indicated by the improved penton stability of the maturation-intermediate mutant, G33A. Full penton destabilization was achieved only when the genome was present *in addition* to the successful maturation-linked proteolytic cleavage of preprotein VI. Therefore these findings indicate that maturation of adenovirus induces penton destabilization and thus, primes the capsid for disassembly. These results emphasize the essential role of penton (in)stability in the capsid disassembly pathway. In cases where the pentons are too well connected to the rest of the capsid as in the immature capsid, they cannot act as effective conduits for disassembly. This means that upon stress either the capsid stays intact or the whole particle falls apart. Both situations are undesirable. In the former case no genome uncoating will occur and in the latter case the genome would be uncoated prematurely during exposure to stress in the endosome and the DNA could be degraded before it reaches the nuclear pore complex. Therefore a pathway to destabilize the penton region in a controlled manner is required. This is done during maturation by cleaving preprotein VI to weaken the penton region. The additional effect of genomic pressure, in concert with the previously observed effects of integrin binding,[25] set the stage for penton removal and successful infection.

Materials and methods

Virus preparation

The viruses used in this study, the mature, wild type (WT) HAdV-C5, the immature light-density particle (IC), and the HAdV-C5 G33A (G33) virus were prepared as described previously.[15,39,40] Briefly, WT-HAdV5 and G33A viruses were propagated in A549 cells that were maintained in DMEM supplemented with 10% fetal bovine serum, 10 mM HEPES, 2 mM L-glutamine, 0.1 mM non-essential amino acids, 100 units per ml penicillin and 100 μg ml^{-1} streptomycin. Viruses were isolated from cell lysates by sequential freeze–thaw cycles fol-

lowed by double banding in cesium chloride ($CsCl_2$) density gradients.[41] Viruses were dialyzed into 40 mM Tris (pH 8.1), 500 mM sodium chloride, 2% (wt/vol) sucrose and 1% (wt/vol) mannitol.

Atomic force microscopy

AFM (Nanotec Electrónica S.L., Madrid, Spain) experiments were performed in solution at room temperature. Approximately 100 μl of the sample investigated (virus concentration of ~10 μg ml^{-1}) was deposited on hydrophobic glass and incubated for 15 minutes. Hydrophobic glasses were prepared as previously described.[29] For nanoindentation experiments, hydrophobic glass cover slips and rectangular, silicon-nitride cantilevers were used with a nominal spring constant and tip radius of 0.1 N m^{-1} and 15 nm, respectively (Olympus OMCL-RC800PSA). For fatigue experiments, mica surfaces and rectangular, silicon-nitride cantilevers with a nominal spring constant and tip radius of 0.05 N m^{-1} and 15 nm, respectively (Olympus OMCL-RC800PSA), were used. Each cantilever was calibrated using the Sader method.[42] To estimate the tip radius for nanoindentation experiments, imaging was performed in contact mode on a ultrananocrystalline diamond (UNCD Aqua 100) surface and the subsequent image was used for blind tip estimation, as described previously.[43]

AFM imaging was performed in Jumping Mode Plus[44] where the maximum scanning force was ~100 pN. Nanoindentations were performed by indenting a virus in its centre with the AFM tip during individual force–distance curve (FDC) experiments. A FDC is also performed on glass in order to calculate the indentation response of the virus (force-indentation curve, FIC). The spring constant of the virus was measured as the slope of the linear regime in the FIC. The break force was measured as the value where the force dramatically drops, indicating capsid disruption. The cumulative probability of penton release was calculated by binning the data of penton release time (bin size = 7.5 minutes) and counting the cumulative number of observations up to the maximum bin size. The cumulative number of observations were then divided into the total number of observations (*i.e.* total number of pentons released) and multiplied by 100.

Conflicts of interest

There are no conflicts of interest to declare.

Acknowledgements

W. H. R. is grateful for financial support through a VIDI grant from the Nederlandse Organisatie voor Wetenschappelijk Onderzoek (NWO) and a FOM projectruimte grant. W. H. R. and G. N. acknowledge funding *via* a NIH R21 grant. G. J. L. W. acknowledges funding *via* a NWO VICI grant and a European Research Council Starting Independent Investigator grant.

References

1 M. A. Kotterman and D. V. Schaffer, Engineering adeno-associated viruses for clinical gene therapy, *Nat. Rev. Genet.*, 2014, **15**, 445–451.
2 J. Flint and G. R. Nemerow, *Human Adenoviruses: From Villains to Vectors*, World Scientific, New Jersey, 2016.
3 N. Kol, Y. Shi, M. Tsvitov, D. Barlam, R. Z. Shneck, M. S. Kay and I. Rousso, A stiffness switch in human immunodeficiency virus, *Biophys. J.*, 2007, **92**, 1777–1783.
4 W. Roos, R. Bruinsma and G. Wuite, Physical virology, *Nat. Phys.*, 2010, **6**, 733–743.
5 A. Ortega-Esteban, G. N. Condezo, A. J. Pérez-Berná, M. Chillón, S. J. Flint, D. Reguera, C. San Martín and P. J. de Pablo, Mechanics of viral chromatin reveals the pressurization of human adenovirus, *ACS Nano*, 2015, **9**, 10826–10833.
6 C. San Martín, Latest insights on adenovirus structure and assembly, *Viruses*, 2012, **4**, 847–877.
7 W. F. Mangel and C. San Martín, Structure, function and dynamics in adenovirus maturation, *Viruses*, 2014, **6**, 4536–4570.
8 P. Ostapchuk and P. Hearing, *In Adenoviruses: Model and Vectors in Virus-Host Interactions*, Springer, 2003, pp. 165–185.
9 P. Ostapchuk and P. Hearing, Control of adenovirus packaging, *J. Cell. Biochem.*, 2005, **96**, 25–35.
10 B. Edvardsson, E. Everitt, H. Jörnvall, L. Prage and L. Philipson, Intermediates in adenovirus assembly, *J. Virol.*, 1976, **19**, 533–547.
11 Y. S. Ahi and S. K. Mittal, Components of Adenovirus Genome Packaging, *Front. Microbiol.*, 2016, **7**, 1503.
12 A. Webster, S. Russell, P. Talbot, W. T. Russell and G. Kemp, Characterization of the adenovirus proteinase: substrate specificity, *J. Gen. Virol.*, 1989, **70**, 3225–3234.
13 T. B. Hasson, D. Ornelles and T. Shenk, Adenovirus L1 52-and 55-kilodalton proteins are present within assembling virions and colocalize with nuclear structures distinct from replication centers, *J. Virol.*, 1992, **66**, 6133–6142.
14 J. Weber, Genetic analysis of adenovirus type 2 III. Temperature sensitivity of processing viral proteins, *J. Virol.*, 1976, **17**, 462–471.
15 C. L. Moyer, E. S. Besser and G. R. Nemerow, A Single Maturation Cleavage Site in Adenovirus Impacts Cell Entry and Capsid Assembly, *J. Virol.*, 2016, **90**, 521–532.
16 C. M. Wiethoff, H. Wodrich, L. Gerace and G. R. Nemerow, Adenovirus protein VI mediates membrane disruption following capsid disassembly, *J. Virol.*, 2005, **79**, 1992–2000.
17 U. F. Greber, M. Willetts, P. Webster and A. Helenius, Stepwise dismantling of adenovirus 2 during entry into cells, *Cell*, 1993, **75**, 477–486.
18 V. S. Reddy and G. R. Nemerow, Structures and organization of adenovirus cement proteins provide insights into the role of capsid maturation in virus entry and infection, *Proc. Natl. Acad. Sci. U. S. A.*, 2014, **111**, 11715–11720.
19 X. Yu, D. Veesler, M. G. Campbell, M. E. Barry, F. J. Asturias, M. A. Barry and V. S. Reddy, Cryo-EM struc-

ture of human adenovirus D26 reveals the conservation of structural organization among human adenoviruses, *Sci. Adv.*, 2017, **3**, e1602670.

20 X. Dai, L. Wu, R. Sun and Z. H. Zhou, Atomic Structures of Minor Proteins VI and VII in the Human Adenovirus, *J. Virol.*, 2017, **91**(34), DOI: 10.1128/JVI.00850-17.

21 I. Ivanovska, P. De Pablo, B. Ibarra, G. Sgalari, F. MacKintosh, J. Carrascosa, C. Schmidt and G. Wuite, Bacteriophage capsids: tough nanoshells with complex elastic properties, *Proc. Natl. Acad. Sci. U. S. A.*, 2004, **101**, 7600–7605.

22 J. Snijder, C. Uetrecht, R. Rose, R. Sanchez-Eugenia, G. Marti, J. Agirre, D. Guérin, G. Wuite, A. Heck and W. Roos, Probing the biophysical interplay between a viral genome and its capsid, *Nat. Chem.*, 2013, **5**, 502–509.

23 M. G. Mateu, *In Structure and Physics of Viruses*, Springer, 2013, pp. 3–51.

24 M. Marchetti, G. Wuite and W. Roos, Atomic force microscopy observation and characterization of single virions and virus-like particles by nano-indentation, *Curr. Opin. Virol.*, 2016, **18**, 82–88.

25 J. Snijder, V. S. Reddy, E. R. May, W. H. Roos, G. R. Nemerow and G. J. Wuite, Integrin and defensin modulate the mechanical properties of adenovirus, *J. Virol.*, 2013, **87**, 2756–2766.

26 A. Ortega-Esteban, K. Bodensiek, C. San Martín, M. Suomalainen, U. F. Greber, P. J. de Pablo and I. A. Schaap, Fluorescence tracking of genome release during mechanical unpacking of single viruses, *ACS Nano*, 2015, **9**, 10571–10579.

27 M. G. van Rosmalen, G. R. Nemerow, G. J. Wuite and W. H. Roos, A single point mutation in precursor protein VI doubles the mechanical strength of human adenovirus, *J. Biol. Phys.*, 2018, **44**, 1–14.

28 G. N. Condezo, R. Marabini, S. Ayora, J. M. Carazo, R. Alba, M. Chillón and C. San Martín, Structures of adenovirus incomplete particles clarify capsid architecture and show maturation changes of packaging protein L1 52/55k, *J. Virol.*, 2015, **89**, 9653–9664.

29 W. H. Roos, How to perform a nanoindentation experiment on a virus, in *Single Molecule Analysis: Methods and Protocols*, 2011, pp. 251–264.

30 M. M. Gibbons and W. S. Klug, Nonlinear finite-element analysis of nanoindentation of viral capsids, *Phys. Rev. E: Stat., Nonlinear, Soft Matter Phys.*, 2007, **75**, 031901.

31 W. H. Roos, K. Radtke, E. Kniesmeijer, H. Geertsema, B. Sodeik and G. J. Wuite, Scaffold expulsion and genome packaging trigger stabilization of herpes simplex virus capsids, *Proc. Natl. Acad. Sci. U. S. A.*, 2009, **106**, 9673–9678.

32 W. Klug, W. Roos and G. Wuite, Unlocking internal prestress from protein nanoshells, *Phys. Rev. Lett.*, 2012, **109**, 168104.

33 A. J. Pérez-Berná, A. Ortega-Esteban, R. Menéndez-Conejero, D. C. Winkler, M. Menéndez, A. C. Steven, S. J. Flint, P. J. de Pablo and C. San Martín, The role of capsid maturation on adenovirus priming for sequential uncoating, *J. Biol. Chem.*, 2012, **287**, 31582–31595.

34 A. J. Pérez-Berná, W. F. Mangel, W. J. McGrath, V. Graziano, J. Flint and C. San Martín, Processing of the L1 52/55k protein by the adenovirus protease: a new substrate and new insights into virion maturation, *J. Virol.*, 2014, **88**, 1513–1524.

35 A. Ortega-Esteban, A. Pérez-Berná, R. Menéndez-Conejero, S. Flint, C. San Martín and P. De Pablo, Monitoring dynamics of human adenovirus disassembly induced by mechanical fatigue, *Sci. Rep.*, 2013, **3**, 1434.

36 S. Strunze, M. F. Engelke, I.-H. Wang, D. Puntener, K. Boucke, S. Schleich, M. Way, P. Schoenenberger, C. J. Burckhardt and U. F. Greber, Kinesin-1-mediated capsid disassembly and disruption of the nuclear pore complex promote virus infection, *Cell Host Microbe*, 2011, **10**, 210–223.

37 S. K. Natchiar, S. Venkataraman, T.-M. Mullen, G. R. Nemerow and V. S. Reddy, Revised Crystal Structure of Human Adenovirus Reveals the Limits on Protein IX Quasi-Equivalence and on Analyzing Large Macromolecular Complexes, *J. Mol. Biol.*, 2018, **430**, 4132–4141.

38 C. J. Burckhardt, M. Suomalainen, P. Schoenenberger, K. Boucke, S. Hemmi and U. F. Greber, Drifting motions of the adenovirus receptor CAR and immobile integrins initiate virus uncoating and membrane lytic protein exposure, *Cell Host Microbe*, 2011, **10**, 105–117.

39 V. S. Reddy, S. K. Natchiar, P. L. Stewart and G. R. Nemerow, Crystal structure of human adenovirus at 3.5 Å resolution, *Science*, 2010, **329**, 1071–1075.

40 M. Iacobelli-Martinez and G. R. Nemerow, Preferential activation of Toll-like receptor nine by CD46-utilizing adenoviruses, *J. Virol.*, 2007, **81**, 1305–1312.

41 V. Reddy, S. Natchiar, L. Gritton, T.-M. Mullen, P. L. Stewart and G. Nemerow, Crystallization and preliminary X-ray diffraction analysis of human adenovirus, *Virology*, 2010, **402**, 209–214.

42 J. E. Sader, J. W. Chon and P. Mulvaney, Calibration of rectangular atomic force microscope cantilevers, *Rev. Sci. Instrum.*, 1999, **70**, 3967–3969.

43 D. Vorselen, E. S. Kooreman, G. J. Wuite and W. H. Roos, Controlled tip wear on high roughness surfaces yields gradual broadening and rounding of cantilever tips, *Sci. Rep.*, 2016, **6**, 36972.

44 A. Ortega-Esteban, I. Horcas, M. Hernando-Pérez, P. Ares, A. Pérez-Berná, C. San Martín, J. Carrascosa, P. De Pablo and J. Gómez-Herrero, Minimizing tip–sample forces in jumping mode atomic force microscopy in liquid, *Ultramicroscopy*, 2012, **114**, 56–61.

